Using multiples to improve the reservoir response via sparse inversion: application to elastic data

Carlos A. N. da Costa*, Federal University of Pará & INCT-GP, Alok K. Soni, Shell India Markets Pvt. Ltd. (formerly Delft University of Technology) and D.J. (Eric) Verschuur, Delft University of Technology

Abstract

In this paper we propose a strategy to estimate the impulse responses from a local target in the subsurface from surface seismic data, as an iterative sparse inversion approach in two steps. The first step is the process to estimate the up- and downgoing wavefields at a specific level nearby the target through Joint Migration Inversion. The second step is an iterative sparse inversion approach, which estimates the impulse responses from the target. The main feature of this strategy is that all multiple scattering in the data is used to enhance the illumination at target level. Currently, the first step has not yet been fully tested and the results shown are obtained only from the second step, using forward modeling and wavefield decomposition to get the up- and downgoing wavefields at the level nearby the target. The numerical tests show that the iterative sparse inversion approach does not require dense sources sampling to estimate the impulse responses from a target below a complex overburden, because of all the extra illumination via multiples.

Introduction

When imaging a target below a complex overburden, the complex propagation and multiple scattering effects complicate the interpretation and characterization of the target (Thorbecke et al., 2004). A good strategy is to first deal with the overburden effects, followed by migration or inversion just in the desired target (local-schemes) such as JMI-res (Berkhout, 2013) or target-oriented full waveform inversion (Staal et al., 2010; Gisolf and van den Berg, 2010; Haffinger et al., 2012). In exploration seismology these local-schemes are important tools for characterizing or monitoring the reservoir.

One of the main challenges for local-schemes is to get the dataset only containing information from the target area in the subsurface below a complex overburden. This process to derive the local response from the target area, where sources and receivers are projected on to a level just above this area, is usually called redatuming.

There are two main methodologies for this redatuming process. The first one is model-driven datuming, where the traveltimes from sources (or receivers) to the chosen datum level in the subsurface are computed from a prior velocity model and used as time shifts in a Kirchhoff-type integral (Berryhil, 1979, 1984, 1986; Schneider, Jr. et al., 1995; Liu and Xu, 2011). These methods have the drawbacks that they can exhibit some extrapolation artifacts from upward or downward continuation of the wavefields and they are velocity dependent, while estimating a correct velocity model in a complex geological setting is difficult. Another drawback is that they usually are not suitable to correct for complex propagation paths including multiple scattering and transmission effects.

The second redatuming methodology comprises the data-driven methods based on cross-correlation/deconvolution (Wapenaar et al., 2004; Wapenaar, 2004; Wapenaar and Fokkema, 2006; Bakulin and Calvert, 2006; Vasconcelos and Snieder, 2008a,b; Bitri et al., 2011; Soni et al., 2012b; van der Neut and Herrmann, 2013; Wapenaar et al., 2013). These methods only use information from the data itself for redatuming, meaning that these methods are velocity independent. However, they are very dependent on the geometry of acquisition, because they requires dense source and dense receiver sampling (Wapenaar and Fokkema, 2006). In principle, the methods based on deconvolution can be effective in removing the spurious events from the estimated target impulse responses, as pointed out by van der Neut (2012).

Here, we propose an approach to estimate the impulse responses for P- and S-wavefields that include every possible wave conversion from a target in two steps, where the velocity model estimation is incorporated and the sampling requirements are less strict. Moreover, all multiple scattering and transmission effects are taken into account, where multiples can help to provide additional angles of illumination at target level. The first step is estimating the up- and downgoing wavefields generated by sources at surface at a desired level in the subsurface with Joint Migration Inversion (JMI) (Berkhout, 2012, 2014b) for P- and S-wavefields. In the JMI approach, at every depth level in the subsurface the up- and downgoing wavefields are estimated (with surface-related and internal multiples), together with the velocity model and the image. The second step is to apply an iterative sparse inversion approach using the up/downgoing wavefields at target level to estimate the impulse responses from the target for both types of wavefields. In this second step, each iteration is a multidimensional deconvolution, similar the acoustic scheme formulated by van der Neut and Herrmann (2013). With this scheme, we expect to redatuming elastic reflection dataset a straightforward and convenient way and overcome spurious events in the elastic impulse responses.

In this study, the JMI process has not been tested yet and the results shown in this paper, are obtained only from the second step, using modeled stressfields and particle velocities at target level followed by an elastic wavefield decomposition to get the up- and downgoing wavefields at a level nearby our target. A similar formulation for the acoustic case, for this second step, has already been investigated by Soni et al. (2012b), for VSP data and van der Neut and Herrmann (2013) for surface data. However, here we will show for the elastic case through numerical examples, that by including all multiples in the wavefields that are used for the deconvolution process, we can relax the source sampling to estimate reliable impulse responses from a target below a complex overburden.

Sparse inversion scheme for converted waves

Using the operator notation in the temporal frequency domain as given in Berkhout (1982), the discrete wavefield for P- and S-waves can be described by the following four monochromatic expressions (Berkhout, 2014a):

$$\mathbf{P}_j^{(\zeta)+}(z_m^-;z_0) = \mathbf{W}^{(\zeta\zeta)+}(z_m^-,z_0)\mathbf{S}_j^+(z_0) + \sum_{n=0}^{m-1}\mathbf{W}^{(\zeta\zeta)+}(z_m^-,z_n^+)\delta\mathbf{S}_j^{(\zeta)+}(z_n^+;z_0), \quad (1)$$

with $m = 1,2,...,M$ and

$$\mathbf{P}_j^{(\zeta)-}(z_m^+;z_0) = \mathbf{W}^{(\zeta\zeta)-}(z_m^+,z_M)\mathbf{P}_j^{(\zeta)-}(z_M;z_0) + \sum_{n=m+1}^{M}\mathbf{W}^{(\zeta\zeta)-}(z_m^+,z_n^-)\delta\mathbf{S}_j^{(\zeta)-}(z_n^-;z_0), \quad (2)$$

with $m = 0,1,...,M-1$ and the superscript ζ indicates P-waves for $\zeta = p$ and S-waves for $\zeta = s$. Here $z_m^{\pm}$ represents the m^{th} depth level in the subsurface where the superscripts + and - indicate underside and upper side at any depth level, respectively, M indicates the number of depth levels on the grid, the elements of vector $\mathbf{S}_j^+(z_0)$ represent the source array with identification label j at the surface z_0. The matrices $\mathbf{W}^{(\zeta\zeta)\pm}(z_m^{\mp},z_n^{\mp})$ represent the downward (with superscript +) and upward (with superscript -) propagation operator between depth levels z_m and z_n for P- and S-waves. In equations 1 and 2, the elements of vectors $\mathbf{P}_j^{(\zeta)\pm}(z_m^{\mp};z_0)$, i.e $P_{ij}^{(\zeta)\pm}(z_m^{\mp};z_0)$, represent the down- (with superscript +) and upgoing (with superscript -) wavefields incident to gridpoint i at depth level $z_m^{\mp}$ that were generated by source array j at depth level z_0 for both type of wavefields. The secondary source vectors $\delta\mathbf{S}_j^{(\zeta)\pm}(z_n^{\pm},z_0)$ are including the transmission and reflection processes at depth level $z_n^{\pm}$, which are given by a linear combination of PP-, PS-, SP- and SS-wavefields coming from of up- and downgoing incident wavefields at $z_n^{\pm}$ (Berkhout, 2014a). These secondary source vectors are given by:

$$\begin{aligned}\delta\mathbf{S}_j^{(\zeta)+}(z_m^+;z_0) =& \sum_i \mathbf{R}_i^{(\zeta\eta)\cap}(z_m^+;z_m^+)\mathbf{P}_{ij}^{(\eta)-}(z_m^+;z_0)\delta_{\eta p+s-\zeta} \\ &+\sum_i \mathbf{R}_i^{(\zeta\zeta)\cap}(z_m^+;z_m^+)\mathbf{P}_{ij}^{(\zeta)-}(z_m^+;z_0) \\ &+\sum_i \delta\mathbf{T}_i^{(\zeta\eta)+}(z_m^+;z_m^-)\mathbf{P}_{ij}^{(\eta)+}(z_m^-;z_0)\delta_{\eta p+s-\zeta} \\ &+\sum_i \delta\mathbf{T}_i^{(\zeta\zeta)+}(z_m^+;z_m^-)\mathbf{P}_{ij}^{(\zeta)+}(z_m^-;z_0) \quad (3)\end{aligned}$$

and

$$\begin{aligned}\delta\mathbf{S}_j^{(\zeta)-}(z_m^-;z_0) =& \sum_i \mathbf{R}_i^{(\zeta\eta)\cup}(z_m^-;z_m^-)\mathbf{P}_{ij}^{(\eta)+}(z_m^-;z_0)\delta_{\eta p+s-\zeta} \\ &+\sum_i \mathbf{R}_i^{(\zeta\zeta)\cup}(z_m^-;z_m^-)\mathbf{P}_{ij}^{(\zeta)+}(z_m^-;z_0) \\ &+\sum_i \delta\mathbf{T}_i^{(\zeta\eta)-}(z_m^-;z_m^+)\mathbf{P}_{ij}^{(\eta)-}(z_m^+;z_0)\delta_{\eta p+s-\zeta} \\ &+\sum_i \delta\mathbf{T}_i^{(\zeta\zeta)-}(z_m^-;z_m^+)\mathbf{P}_{ij}^{(\zeta)-}(z_m^+;z_0). \quad (4)\end{aligned}$$

Where $\delta_{\eta p+s-\zeta}$ is the Kronecker delta, the vectors $\mathbf{R}_i^{\cap}(z_m^+;z_m^+)$ and $\mathbf{R}_i^{\cup}(z_m^-;z_m^-)$ represent the angle-dependent reflection operators at level z_m for all type of wavefields ($\mathbf{R}_i^{(pp)}$, $\mathbf{R}_i^{(ss)}$, $\mathbf{R}_i^{(sp)}$ and $\mathbf{R}_i^{(ps)}$). The operator $\mathbf{R}_i^{\cap}(z_m^+;z_m^+)$ transforms up- into downgoing wavefield and $\mathbf{R}_i^{\cup}(z_m^-;z_m^-)$ transforms down- into upgoing wavefield. The vectors $\delta\mathbf{T}_i^-(z_m^-;z_m^+)$ and $\delta\mathbf{T}_i^+(z_m^+;z_m^-)$ represent the angle-dependent transmission operators at level z_m for up-dan downgoing wavefields, respectively for all types of wavefields ($\delta\mathbf{T}_i^{(pp)}$, $\delta\mathbf{T}_i^{(ss)}$, $\delta\mathbf{T}_i^{(sp)}$ and $\delta\mathbf{T}_i^{(ps)}$). Note that the above expressions are including every possible wave conversion.

At each depth level z_m we can also link the down- and upgoing wavefields from equation 2 as follows:

$$\begin{aligned}P_{kj}^{(\zeta)-}(z_m^+;z_0) &= \sum_i X_{ki}^{(\zeta p)}(z_m^+,z_m^+)\delta S_{ij}^{(p)+}(z_m^+;z_0) \\ &+ \sum_i X_{ki}^{(\zeta s)}(z_m^+,z_m^+)\delta S_{ij}^{(s)+}(z_m^+;z_0), \quad (5)\end{aligned}$$

where $X_{ki}^{(\zeta\gamma)}(z_m^+,z_m^+)$ represents the impulse response from an area below depth level z_m^+, generated by downgoing P- and S-wavefields at gridpoint i and observed at gridpoint k at depth level z_m^+ for P- and S-wavefields, in the frequency domain. Note that in equation 5, are used all kinds of scattered wavefields (surface-related and internal multiples) and every posible conversion (PS and SP) wavefields that are observed at gridpoint i as effective source wavefield for obtaining the complete upgoing wavefield $P_{kj}^{(\zeta)-}(z_m^+;z_0)$. With this in mind, it is interesting to realize that the more complex the overburden above level z_m, the richer the illumination will be for the area below this level.

Assuming that we have the up- and downgoing wavefields at a target level z_d, a way to estimate the impulse responses at that level is to estimate the inverse of the equation 5 (van Groenestijn and Verschuur, 2008, 2009, 2010; Soni et al., 2012b; van der Neut and Herrmann, 2013). We use an iterative solution to reverse this equation based in the least-squares inversion method. Our iterative inversion scheme is minimizing the difference between the total upgoing wavefield recorded at target level, $\mathbf{P}_j^{(\zeta)-}(z_d;z_0)$, and the predicted upgoing wavefield via the estimated impulse responses at the same level, i.e. the residual $\Delta\mathbf{P}_j^{(\zeta)}(z_d)$:

$$\begin{aligned}\Delta\mathbf{P}_j^{(\zeta)}(z_d) &= \mathbf{P}_j^{(\zeta)-}(z_d;z_0) - \sum_i \hat{\mathbf{X}}_i^{(\zeta p)}(z_d,z_d)\delta S_{ij}^{(p)+}(z_d;z_0) \\ &- \sum_i \hat{\mathbf{X}}_i^{(\zeta s)}(z_d,z_d)\delta S_{ij}^{(s)+}(z_d;z_0), \quad (6)\end{aligned}$$

where $\hat{}$ indicates that it is an estimated value. To drive the residual, equation 6, to zero, we minimize the following objective function:

$$J_{ls}^{(\zeta)} = \left(\frac{1}{\sigma_n^2}\right) \sum_{\omega} ||\Delta \mathbf{P}_j^{(\zeta)}(z_d)||_F^2, \quad (7)$$

where the parameter σ_n is a data weight, ω is the temporal frequency and the underscript F indicates the Frobenius norm of the residual (Golub and van Loan, 1996).

In general this inversion problem must be regularized. In this work, we use a constraint that promotes sparsity on the estimated impulse responses in the time domain. Sparsity here means that the estimated impulse responses in the time domain, preferably consist of a series of large spikes. This sparsity can be found with any non-quadratic regularization term that penalizes the typical smearing of energy from quadratic norm (in the our case, Frobenius norm) and favor sparsity (Wiggins, 1978; van Groenestijn and Verschuur, 2008, 2009, 2010; Soni et al., 2012a,b). Here we use a mixed $l_1 - l_2$ norm, given by:

$$J_{reg}^{(\zeta)} = \sum_t \sum_{i,j} \sqrt{1 + \frac{\hat{x}_{ij}^{(\zeta p)2}}{\sigma_x^2}} + \sum_t \sum_{i,j} \sqrt{1 + \frac{\hat{x}_{ij}^{(\zeta s)2}}{\sigma_x^2}}, \quad (8)$$

where t represents time, the parameter σ_x is a model weight, $\hat{x}_{ij}^{(\zeta\gamma)}$ denotes an element of the estimated impulse responses matrix $\hat{\mathbf{x}}^{(\zeta\gamma)}$ in the time domain. Further, a time-window is placed over the update of $\hat{\mathbf{x}}^{(\zeta\gamma)}$ in the time domain to impose causality and select the desired arrivals.

With the sparsity constraint, equation 8, we get the following constrained objective function:

$$J^{(\zeta)(n)} = J_{ls}^{(\zeta)(n)} + \varepsilon^2 J_{reg}^{(\zeta)(n)}, \quad (9)$$

where ε is weighting applied to the constraint in the minimization process and superscript n represents the n^{th} iteration.

We used the descent iterative optimization process to solve the above minimization problem, where the descent direction is given by minus of the gradient of the equation 9. This gradient is given by:

$$\nabla_{\zeta\gamma} J^{(\eta)(n)} = \nabla_{\hat{\mathbf{X}}_{\zeta\gamma}} J_{ls}^{(\eta)(n)} + \varepsilon^2 \nabla_{\hat{\mathbf{x}}_{\zeta\gamma}} J_{reg}^{(\eta)(n)}, \quad (10)$$

where the matrix $\nabla_{\hat{\mathbf{X}}^{(\zeta\gamma)}} J_{ls}^{(\eta)}$ is given by:

$$\nabla_{\hat{\mathbf{X}}_{\zeta\gamma}} J_{ls}^{(\eta)} = -\left(\frac{1}{\sigma_n^2}\right) \sum_{\omega} \left[\Delta \mathbf{P}_j^{(\eta)}(z_d) \left(\delta \mathbf{S}^{(\gamma)+}(z_d; z_0)\right)^{\dagger}\right], \quad (11)$$

where superscript † indicates the complex adjoint of $\delta \mathbf{S}^{(\gamma)+}$, i.e. the complex conjugate of the transposed matrix and each element of the matrix $\nabla_{\hat{\mathbf{X}}^{(\zeta\gamma)}} J_{reg}^{(\eta)}$ is given by:

$$\frac{\partial J_{reg}^{(\eta)}}{\partial x_{lm}^{(\zeta\gamma)}} = \sum_t \frac{\hat{x}_{lm}^{(\zeta\gamma)(n)}}{\sqrt{\sigma_x^4 + \sigma_x^2 \hat{x}_{lm}^{(\zeta\gamma)(n)2}}}, \quad (12)$$

With this descent direction we can estimate the target impulse responses as an iterative process with its update in every iteration n given by:

$$\hat{\mathbf{X}}^{(\zeta\gamma)(n+1)} = \hat{\mathbf{X}}^{(\zeta\gamma)(n)} + \alpha^{(\zeta\gamma)(n)} \Delta \hat{\mathbf{X}}^{(\zeta\gamma)(n)}, \quad (13)$$

where $\hat{\mathbf{X}}^{(\zeta\gamma)(n+1)}$ indicates the update of the estimated impulse responses for the n^{th} iteration, $\Delta \hat{\mathbf{X}}^{(\zeta\gamma)(n)} \equiv -\nabla_{\zeta\gamma} J^{(\eta)}$ is the descent direction and $\alpha^{(\zeta\gamma)(n)}$ is frequency and time independent step length that scales the update. This step length must be chosen such that the constrained objective function value, see equation 9, decreases for every iteration, i.e. $J^{(\eta)(n+1)} < J^{(\eta)(n)}$. In the first iteration of this algorithm, we set the values of $\hat{\mathbf{X}}^{(\zeta\gamma)(1)}$ to be zero.

Numerical results

The effect of the proposed inversion scheme will be demonstrated on one synthetic dataset. The synthetic dataset was simulated with an elastic Finite Difference algorithm using a Ricker pulse as wavelet and considering 13.0 Hz as peak frequency. To generate this synthetic dataset we used one elastic model spanning 6000 m in the lateral direction and 1300 m in depth with a very complex overburden, displayed in Figure 1, which has a and it has free-surface on top. The model contains a target area, consisting of two horizontal reflectors. As a datum level we will consider $z_d = 700$, just above these two reflectors.

The up- and downgoing wavefields for synthetic dataset was estimated through extracting the stressfields (T_{xz} and T_{zz}) and particle velocities (V_x and V_z) at target level and applying an elastic wavefield decomposition (Schalkwijk, 2001). We used 201 sources located at surface $z_0 = 0$ m, positioned from x=1000 m to x=5000 m, with increments of 20 m and we used 201 receivers located at depth level $z_d = 700$ m (target level) from x=1000 m to x=5000 m, with increments of 20 m. Figure 2 shows for a source positioned at the surface at x = 3000 m, the down- (on the left side) and upgoing (on the right side) wavefields for P- (on the top) and S-waves (on the bottom). For that model, the estimated impulse responses, at target level $z_d = 700$ m, should exhibit at least two events.

Next, we carry out our inversion scheme using the up/downgoing wavefields for a varying number source responses. First, we use all 201 source locations at the surface. Figures 3 and 4 display the estimated impulse responses (on the right side) for P- and S-waves, respectively, after 30 iterations of the inversion scheme with sparsity constraint (on the bottom) and without sparsity constraint (on the top), from a virtual source positioned at target level, x = 3000 and $z_d = 700$ m. As expected, we observe the two target reflections events, but other than result without sparsity constraint, the result with sparsity constraint has high resolution and few noticeable artifacts. Further, we can observe a good agreements between the estimated (on the the center) and the measured upgoing wavefields (on the left side) for both results. Also note that all AVO effects due to angle-dependent reflections at the target reflections have been recovered. Thus, these estimated impulse responses can serve as input for a local reservoir characterization process.

Next, we will investigate how these results depend on the source sampling. We can see that the wavefields displayed in Figure 2 for P and S-waves, that up and downgoing wavefields exhibit a large amount of complex events due the complex overburden. This will provide a rich illumination at target level $z_d = 700$ m from all downgoing events. Thus we expect that we can use less dense source sampling to estimate the impulse responses than the first results shown in Figures 3 and 4. This observation is

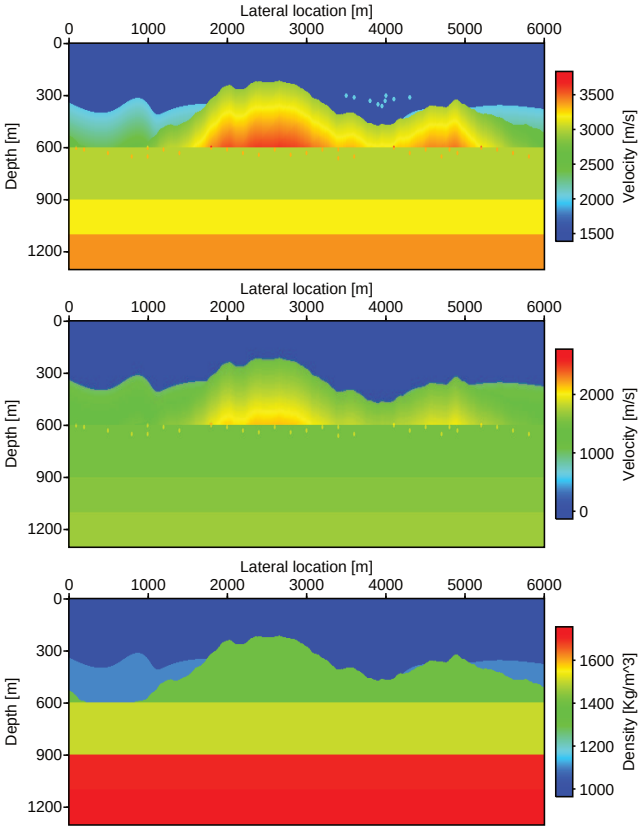

Figure 1: Elastic parameters used to generate elastic synthetic data. Top: v_p velocity model. Middle: v_s velocity model. Bottom: density model.

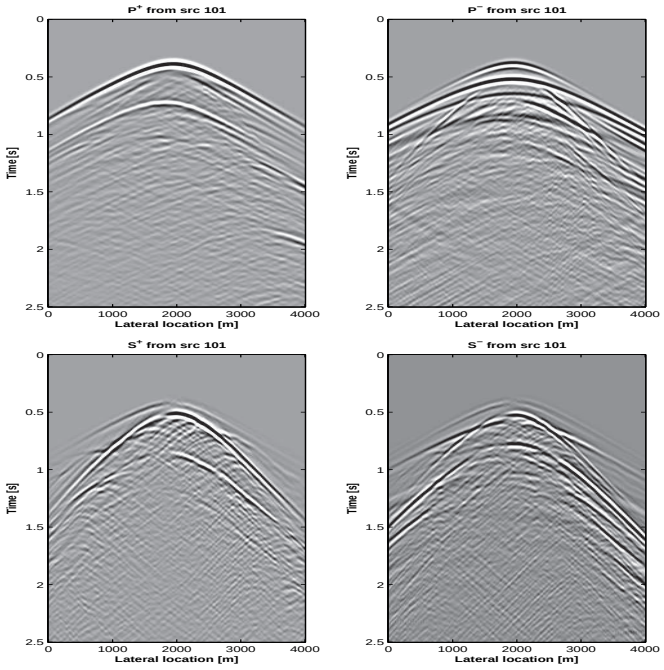

Figure 2: Wavefields for P-waves (on the top) and S-waves (on the bottom) at depth level 700 m from a source positioned at the surface at x=3000 m. Left: downgoing wavefield. Right: upgoing wavefield.

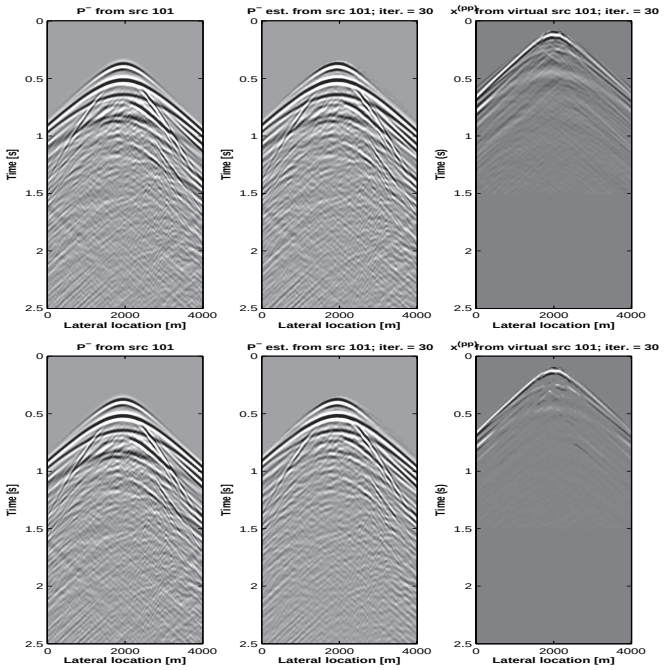

Figure 3: Estimated impulse responses after 30 iterations without sparsity constraint (on the top) and with sparsity constraint (on the bottom) for P-waves from a virtual source positioned at x=3000 m. Left: measured upgoing wavefield. Center: estimated upgoing wavefield. Right: estimated PP impulse responses.

confirmed in the results shown in Figures 5 and 6 for P and S-waves, respecitely, which displays the results of the sparse inversion scheme after 30 iterations for two factors (2 and 4) of decimation of sources. Despite that the resolution decreases for both results, with increasing decimation factor (from top to bottom), we note that the estimated impulse responses for both types of waves still exhibit the two events and we can observe that a good agreement between the estimated (on the center) and the measured upgoing wavefields (on the left side) for both results is observed.

Conclusions

In this paper we discuss one part of the complete JMI strategy for characterizing a certain target area (e.g. the reservoir). The JMI process can generate the up- and downgoing wavefields at any level in the subsurface. In order to more accurately analyze and evaluate a specific target area, it was shown that with a dedicated inversion process the impulse responses from the target area at a level just above this zone can be estimated in a reliable manner. Once these impulse responses have been optimally estimated, they can be used as input for localized inversion processes, like full bandwidth, full waveform inversion.

The inversion process aims at finding the impulse responses such that, when applied to the downgoing wavefields at the target level, the corresponding upgoing wavefields are explained. Furthermore, extra constraints are included to regularize the problem, like causality and

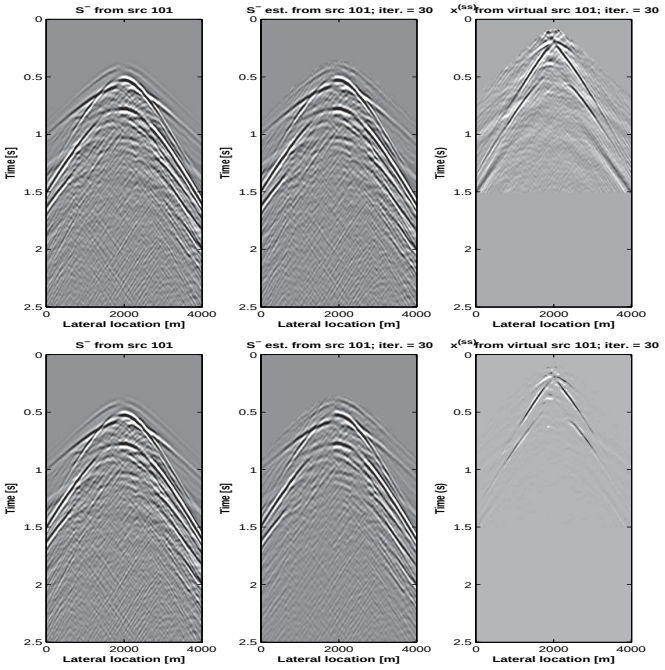

Figure 4: Estimated impulse responses after 30 iterations without sparsity constraint (on the top) and with sparsity constraint (on the bottom) for S-waves from a virtual source positioned at x=3000 m. Left: measured upgoing wavefield. Center: estimated upgoing wavefield. Right: estimated SS impulse responses.

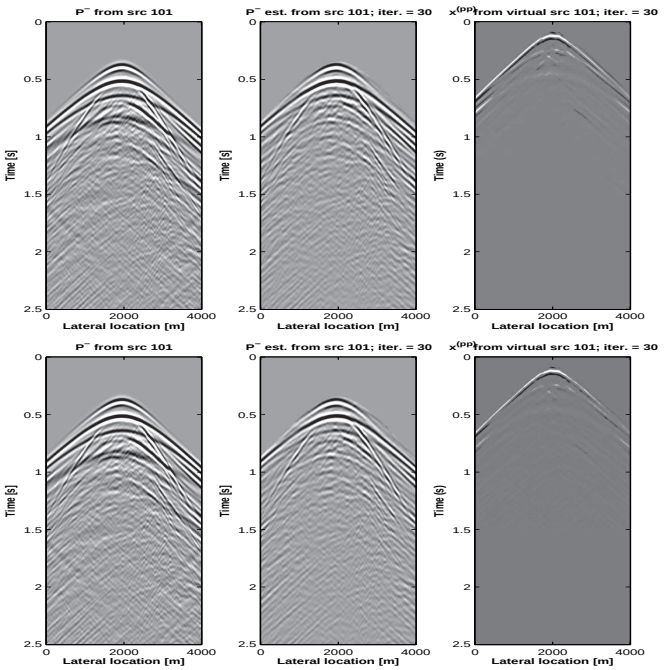

Figure 5: Estimated PP impulse responses after 30 iterations from a virtual sources positioned at x=3000 m, for two different decimation factors. Top: factor 2. Bottom: factor 4.

sparsity.

The results showed that our algorithm worked very well

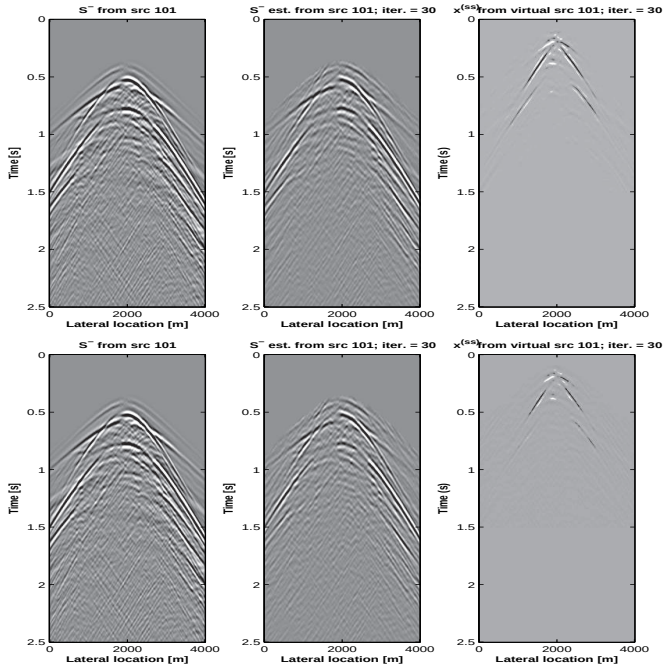

Figure 6: Estimated SS impulse responses after 30 iterations for from a virtual sources positioned at x=3000 m, for two different decimation factors. Top: factor 2. Bottom: factor 4

for elastic data, indicating that it is an effective scheme to estimate elastic impulse responses from a local target from up- and dowgoing wavefields at the target level. These results showed that for a model with a complex overburden, this scheme is very robust to estimate impulse responses for a target area below this complex overburden, because in this case, the illumination is richer due the scattering into overburden and surface multiples. This means that using all multiples in the inversion process will relax the requirement of dense source sampling at the surface, making this a feasible process in realistic 3D acquisition geometries. Furthermore, a more complex overburden can provide a much better illumination of the target area in terms of providing all angles of incidence at the target.

ACKNOWLEDGMENTS

The authors thank the sponsors of the Delphi consortium for their support as well as scholarship from CAPES-Proc. n^o : 99999.003703/2014 – 02, the Project INCT-GP and the Brazilian research agency FINEP.

References

Bakulin, A., and Calvert, R., 2006, The virtual source method: Theory and case study: Geophysics, **71**, no. 4, SI139–SI150.

Berkhout, A. J., 1982, Seismic migration, imaging of acoustic energy by wave field extrapolation, Part A: theoretical aspects: Elsevier.

Berkhout, A. J., 2012, Combining full wavefield migration and full waveform inversion, a glance into the future of seismic imaging: Geophysics, **77**, no. 2, S43–S50.

Berkhout, A. J., 2013, The road ahead in seismic

processing: 83th Ann. Internat. Mtg., Soc. Expl. Geophys., Expanded abstracts, 4488–4492.

Berkhout, A. J., 2014a, Review paper: An outlook on the future seismic imaging, part I: forward and reverse modelling: Geophysical Prospecting, **62**, no. 5, 911–930.

Berkhout, A. J., 2014b, Review paper: An outlook on the future seismic imaging, part III: Joint Migration Inversion: Geophysical Prospecting, **62**, no. 5, 950–971.

Berryhil, J. R., 1979, Wave-equation datuming: Geophysics, **44**, no. 8, 1329–1344.

Berryhil, J. R., 1984, Wave-equation datuming before stack: Geophysics, **49**, no. 11, 2064–2066.

Berryhil, J. R., 1986, Submarine canyons: Velocity replacement by wave-equation datuming before stack: Geophysics, **51**, no. 8, 1572–1579.

Bitri, A., Grandjean, G., and Samyn, K., 2011, Surface wave interferometry by crosscorrelation and deconvolution: First Break, **29**, 83–86.

Gisolf, A., and van den Berg, P. M., 2010, Target-oriented non-linear inversion of time-lapse seismic data: 80th Ann. Internat. Mtg., Soc. Expl. Geophys., Expanded abstracts, 2860–2864.

Golub, G. H., and van Loan, C. F., 1996, Matrix computations: The Johns Hopkins University Press.

Haffinger, P., Gisolf, D., and van den Berg, P., 2012, Nonlinear full waveform inversion for high resolution quantitative property estimation: 82nd Ann. Internat. Mtg., Soc. Expl. Geophys., Expanded abstracts, 1–5.

Liu, W., and Xu, F., 2011, Wave-equation global datuming: 81st Ann. Internat. Mtg., Soc. Expl. Geophys., Expanded abstracts, 3414–3418.

Schalkwijk, K. M. N., 2001, Decompositionn of multicomponent ocean-bottom data into P- and S-waves: Ph.D. thesis, Delft University of Technology.

Schneider, Jr., W. A., Phillip, L. D., and Paal, E. F., 1995, Wave-equation velocity replacement of the low-velocity layer for overthrust-belt data: Geophysics, **60**, no. 2, 573–579.

Soni, A. K., Staal, X. A., and Verschuur, D. J., 2012a, VSP imaging using all multiples: Full wavefield migration approach: 82nd Ann. Internat. Mtg., Soc. Expl. Geophys., Expanded abstracts, 1–6.

Soni, A. K., Woutersand, W., and Verschuur, D. J., 2012b, Target oriented vsp imaging - a sparse-inversion approach: 74th Conference & Exhibition, Expanded abstracts.

Staal, X. R., Verschuur, D. J., Gisolf, A., Tonellot, T., and Burnstad, R., 2010, Improved target-oriented linear full waveform inversion: 72nd Conference & Exhibition, Expanded abstracts.

Thorbecke, J. W., Wapenaar, K., and Swinnen, G., 2004, Design of one-way wavefield extrapolation operators, using smooth functions in wlsq optimization: Geophysics, **69**, no. 4, 1037–1045.

van der Neut, J., and Herrmann, F. J. J., 2013, Interferometric redatuming by sparse inversion: Geophysical Journal International, **192**, 666–670.

van der Neut, J., 2012, Interferometric redatuming by multidimensional deconvolution: Ph.D. thesis, Delft University of Technology.

van Groenestijn, G. J. A., and Verschuur, D. J., 2008, Towards a new approach for primary estimation: 78th Ann. Internat. Mtg., Soc. Expl. Geophys., Expanded abstracts, 2487–2491.

van Groenestijn, G. J. A., and Verschuur, D. J., 2009, Estimating primaries by sparse inversion and application to near-offset data reconstruction: Geophysics, **74**, no. 3, A23–A28.

van Groenestijn, G. J. A., and Verschuur, D. J., 2010, Estimating primaries by sparse inversion from passive seismic data: Geophysics, **75**, no. 4, SA61–SA69.

Vasconcelos, I., and Snieder, R., 2008a, Interferometry by deconvolution, part 1- theory for acoustic waves and numerical examples: Geophysics, **73**, no. 3, S115–S128.

Vasconcelos, I., and Snieder, R., 2008b, Interferometry by deconvolution: Part 2 - theory for elastic waves and application to drill-bit seismic imaging: Geophysics, **73**, no. 3, S129–S141.

Wapenaar, K., and Fokkema, J., 2006, Green's function representations for seismic interferometry: Geophysics, **71**, no. 4, SI33–SI46.

Wapenaar, K., Thorbecke, J., and Draganov, D., 2004, Relations between reflection and transmission responses of three-dimensional inhomogeneous media: Geophysical Journal International, **156**, 179–194.

Wapenaar, K., Slob, E., van der Neut, J., Thorbecke, J., Broggini, F., and Snieder, R., 2013, Three-dimensional marchenko equation for green's function retrieval "beyond seismic interferometry": 83rd Ann. Internat. Mtg., Soc. Expl. Geophys., Expanded abstracts, 4573–4578.

Wapenaar, K., 2004, Retrieving the elastodynamic gree's function of an arbitrary inhomogeneous media by cross correlation: Physical Review Letters, **93**, no. 254301.

Wiggins, R. A., 1978, Minimum entropy deconvolution: Geoexploration, **16**, 21–35.